Finite element analysis of the Reynolds lubrication equation with cavitation

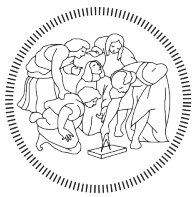

POLITECNICO
MILANO 1863

Simone Nati Poltri, Lorenzo Vallisa

NUMERICAL ANALYSIS FOR PARTIAL DIFFERENTIAL EQUATIONS

Professor: Paola Francesca Antonietti
Supervisors: Nicola Parolini, Marco Verani

12/09/2019

Contents

1 Physical introduction

1.1 Cavitation

Liquids may encounter instabilities when they are subject to deep pressure drops: vapour tension of the liquid reaches the same value of the ambient pressure, causing surface tensions among different phase structures to become not negligible anymore. Indeed this phenomenon gives rise to formation of bubbles within the liquid.
This phenomenon can be further classified into *gaseous* and *vaporeous cavitation*. The former happens when the pressure value reaches the one of the dissolved gas within the liquid. This not being of any harm for the surrounding structure, since the cavitation layer is absorbed into the liquid, not causing any consistent energy release.
The latter instead occurs when the pressure value reaches the liquid tension pressure, generating cavitation bubbles. According to the Gibbs free energy law, the lower the pressure level, less energy is necessary for bubbles to freely expand. At the bubble interface the pressure discontinuity is such to generate the collapse of the bubble structure, whose energy release gives rise to stresses in the order of 1.5 GPa, as it is shown by the blue circle in Figure 1.

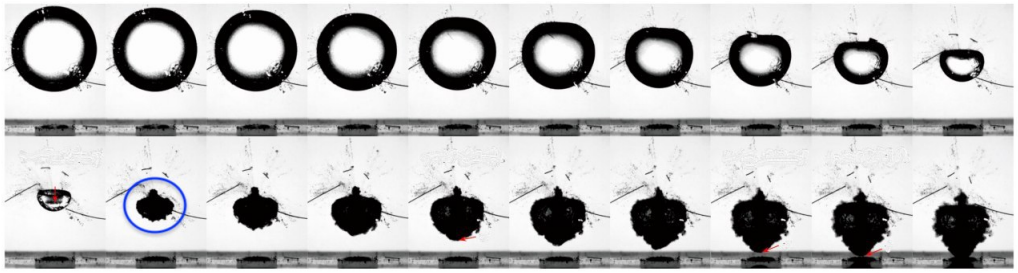

Figure 1: Bubble collapse

1.2 Engineering application

Many are the fields of interest concerning the issue of cavitation: indeed every engineering application that has to deal with hydrodynamics and very high thermal stresses. More specifically in this reference case, hydrodynamics field will be handle, as far as bearings interaction with lubricants is concerned.

Bearings are metallic spheres commonly placed between two structures, as shown on the left part of Figure 2, in order to introduce a rotating degree of freedom. Although, being bearings made of solid materials, contact with outer and inner structures is unavoidable, causing the need of a lubricant oil to be used so as to reduce the generated friction. The right side of Figure 2 shows instead damage caused by the formation and explosion of cavitation bubbles in the above mentioned lubricant film.

Figure 2: Cavitation damage around bearings

1.3 Reynolds equation

As developped in [4], the equation used to describe lubricant behaviour is derived from a simplification of the Navier-Stokes equation for compressible fluids:

$$\rho\left[\frac{\partial \mathbf{u}}{\partial t} + \mathbf{u}\cdot\nabla\mathbf{u}\right] = -\nabla p + \nabla\cdot\mu(\nabla\mathbf{u} + (\nabla\mathbf{u})^T) + \nabla(\lambda\nabla\cdot\mathbf{u}) + \rho\mathbf{f} \qquad (1.1)$$

$$\frac{\partial \rho}{\partial t} + \nabla\cdot(\rho\mathbf{u}) = 0 \qquad (1.2)$$

defined in a bounded domain $\Omega \subset \mathbb{R}^3$.

Some assumptions, in order to rearrange equations (1.1) and (1.2), are needed to face the considered problem. First of all, the gravitational term can be neglected since in cavitation, inertial and viscous terms are much more relevant. Due to the bearings small curvature assumption, cartesian coordinates can be adopted to model the phenomenon, instead of the cylindrical ones. Velocities magnitude in this reference case are such that, not only spatial and

time variation of density are negligible at liquid level (incompressibility assumption), but are not relevant enough for the kinetic energy to overcome the energy connected to viscous effect ($Re \ll 1$). Eventually, taking y coordinate as the one representing film thickness and x and z forming the orthogonal plane to it, in thin fluid modelling the further hypothesis of x and z velocity components much grater than the one along the y axis, holds valid. Equation (1.1) and (1.2) reduce (by components) to:

$$\frac{\partial p}{\partial x} = \mu \frac{\partial^2 u}{\partial y^2} \tag{1.3}$$

$$\frac{\partial p}{\partial y} = 0 \tag{1.4}$$

$$\frac{\partial p}{\partial z} = \mu \frac{\partial^2 w}{\partial y^2} \tag{1.5}$$

$$\frac{\partial u}{\partial x} + \frac{\partial v}{\partial y} + \frac{\partial w}{\partial z} = 0. \tag{1.6}$$

Being pressure constant along y axis, next step is to integrate equations (1.3) and (1.5) along y direction, considering the following boundary conditions: U_2 and W_2 values respectively of u and w at $y = D$ (film thickness), whereas U_1 and W_1 values respectively of u and w at $y = 0$. u and w components are as follows

$$u = \frac{1}{2\mu} \frac{\partial p}{\partial x}(y^2 - Dy) + \frac{U_2 - U_1}{D} y + U_1 \tag{1.7}$$

$$w = \frac{1}{2\mu} \frac{\partial p}{\partial z}(y^2 - Dy) + \frac{W_2 - W_1}{D} y + W_1. \tag{1.8}$$

Plugging into continuity equation (1.6), supposing that bearings are not moving along y directions and eventually integrating the obtained equation along y axis, the final expression of the Reynolds equations, as suggested by [1], yields to:

$$-\nabla \cdot (D^3 \nabla p) = 6\mu U \frac{\partial D}{\partial x}. \tag{1.9}$$

Introducing film characteristic thickness D_* and bearing's characteristic length L_x, equation (1.9) can be further adimensionalized with the following:

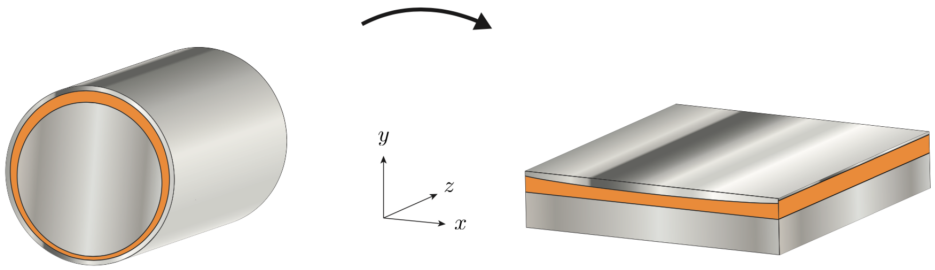

Figure 3: Reference system simplification

$$d = \frac{D}{D_*}, \quad x = \frac{X}{L_x}, \quad p = \frac{L_x D_*^2}{6\mu U} P, \quad \nu = d^3, \quad f = \frac{\partial d}{\partial x} \tag{1.10}$$

resulting in

$$-\nabla \cdot (\nu \nabla p) = f. \tag{1.11}$$

2 Mathematical model

2.1 Functional setting and model

For this reference case the domain structure is subdivided into two main parts: the one in which the fluid is in contact with atmospheric pressure and the one representing the periodical behaviour of the fluid around the bearing. For the first one Dirichlet boundary conditions are adopted, since pressure has to be equal to the atmospheric one when liquid is in contact with air; whereas in the other part of the boundary, periodic condition are enforced to emphasize continuity of the information between Γ_1 and Γ_2 in Figure 4.

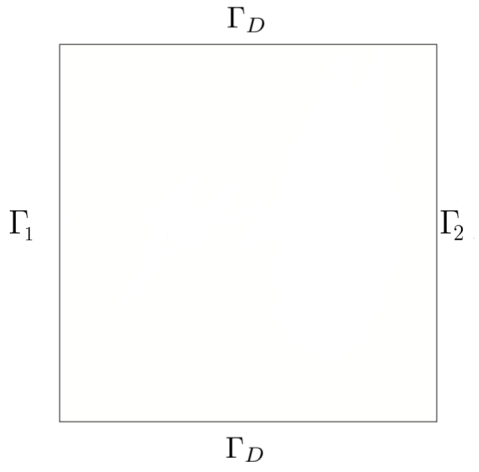

Figure 4: Boundary of the domain

Holding the hypothesis of absence of shock waves (incompressibility), a sufficient regularity of the solution can be assumed ($p \in C^2(\Omega)$) and the continuity can be applied to pressure variable and its gradient along periodic domain. Hence, as far as weak formulation is concerned, the space H^1, denoting an Hilbert space equipped with the associated norm $|| \cdot ||_1$, can be adopted to describe the generic functional setting. More into detail, a subspace of $H^1(\Omega)$ will be used to take in consideration the zero value of the pressure along the Dirichlet boundary:

$$Q = \{q \in H^1(\Omega) \text{ s.t. } q|_{\Gamma_D} = 0\}.$$

Setting Q as space for test functions, the weak formulation begins as follows:

$$\int_\Omega -\nabla \cdot (\nu \nabla p) q = \int_\Omega f q \quad \forall q \in Q. \tag{2.1}$$

Using first Green identity, the following form is recovered:

$$\int_\Omega \nu \nabla p \cdot \nabla q - \int_{\partial\Omega} (\nu \nabla p \cdot \mathbf{n}) q = \int_\Omega f q \quad \forall q \in Q. \tag{2.2}$$

Thanks to continuous differentiability property of pressure and to the test functional setting, equation (2.2) reduces to:

$$a(p, q) = (f, q) \quad \forall q \in Q \tag{2.3}$$

where:

$$a(p, q) := \int_\Omega \nu \nabla p \cdot \nabla q$$

and ν is a smooth, positive and bounded function in Ω.

The presented model is not faithful to the physical phenomenon of the reference case though, since numerical results show unrealistic drops of pressure way below the cavitation value, causing a wrong estimate of the cavitation area itself.

2.2 Obstacle problem

One way to tackle the beforehand mentioned issue is to include the information of pressure non-negativity into the variational formulation, by seeking a solution in a closed convex subset $K \subset Q$:

$$K := \{q \in Q \text{ s.t. } q \geq \psi \text{ a.e. in } \Omega\}$$

where ψ is the cavitation pressure.
Let $(\cdot, \cdot)$ denote the scalar product and $||\cdot||$ the associated norm in the Hilbert space H. The problem can be structured as a *variational inequality problem*, as thoroughly explained in [2], in which, defining the quadratic functional J as

$$J(p) = \frac{1}{2} a(p, p) - (f, p) \quad f \in Q^*, \quad p \in Q \tag{2.4}$$

a minimum of this functional exists and belongs to K if the following variational inequality holds:

$$< J'_G(p), q - p >_* = a(p, q - p) - (f, q - p) \geq 0 \quad \forall q \in K. \tag{2.5}$$

Suppose now $\omega \in Q$ is the unique solution of the variational problem (2.3), such that

$$a(p, q - p) \geq (f, q - p) = a(\omega, q - p)$$

yielding thus

$$a(p - \omega, q - p) \geq 0 \quad \forall q \in K. \tag{2.6}$$

Recalling moreover that the bilinear form a is continuous and positive definite, the norm $|| \cdot ||_Q := \sqrt{a(\cdot, \cdot)}$ can be instead used in the variational inequality formulation. Then (2.6) is equivalent to find

$$\min_{q \in K} ||\omega - q||_Q \tag{2.7}$$

that, according to the projection theorem onto a convex set, is furthermore equivalent to find the projection of $\omega \in Q$ onto K.

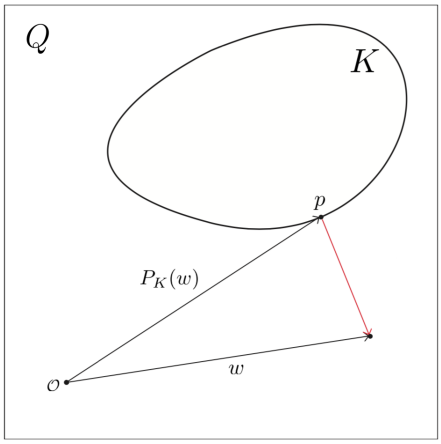

Figure 5: Projected solution of Q onto K

One way to analytically exploit this result is to introduce a penalty operator defined as

$$\beta(\omega) := \omega - P_K(\omega), \quad \omega \in Q. \tag{2.8}$$

Defining furthermore the symmetric, elliptic and continous bilinear form

$$b(p,q) = \int_\Omega \nu p q$$

the condition (2.8) is forced into equation (2.6) as follows:

$$a(p,q) + \frac{1}{\epsilon} b(\beta(p), q) = (f,q) \quad \forall q \in Q \tag{2.9}$$

with $\epsilon \in \mathbb{R}_+$ being the penalty parameter.

Solving (2.9) for p is the so called *obstacle problem* for equality constraints, whose methodology is fully described in [5], in which boundary conditions are forced into the main equation through a penalty parameter. The enforced conditions are not straight the pointwise inequality of pressure variable mentioned while defining the subspace K, but through the obstacle problem the new condition to be satisfied is the equality constraint (2.8), connected thus to the projected solution that is aimed to be found. That is, letting $\epsilon \to 0$, the solution of the initial variational problem (2.3) ω converges to its projection $P_K(\omega)$ onto the subspace K of Q. Indeed the aimed result of (2.9) will be

$$P_K(\omega) = \omega = p.$$

Summing up, the solution of the obstacle problem is equivalent to the solution of equation (2.3), subjected to following constraints:

$$\begin{cases} -\nabla \cdot (\nu \nabla p) - f \geq 0 & in\ \Omega \\ p \geq \psi & in\ \Omega \\ (p-\psi)(-\nabla \cdot (\nu \nabla p) - f) = 0 & in\ \Omega \\ p = 0 & on\ \Gamma_D \\ (p-\psi)\nu \frac{\partial p}{\partial n} = 0 & on\ \Gamma_N \\ p = \psi & on\ \partial\Omega_c \end{cases}$$

where $\partial\Omega_c$ is defined as the boundary of the contact area.

3 Numerical Model

3.1 Finite element formulation

The main purpose is to find a numerical approximation of the solution of equation (2.9), using finite element method. More in details, assuming that the solution has suffiecient regularity, that is $p \in \mathcal{C}^2(\Omega)$, as assumed in [1], continuous Galerkin method has been adopted.
In order to build a numerical formulation of the main problem, it is mandatory to introduce a finite element space

$$Q_h := \left\{ q \in Q \text{ s.t. } q|_T \in \mathbb{P}^1(T) \ \forall T \in \mathcal{T}_h \right\} \subset Q$$

denoting with $\mathcal{T}_h$ a regular partitioning of Ω into uniform three-node regular triangular elements of mesh size h and with $\mathbb{P}^1$ the set of all polynomials of degree one.

Knowing the behaviour of the projected solution ω onto K, defined through the pointwise inequality $p \geq \psi$, the real unknown, beside the value of p itself, is the region of the domain $\Omega_{c,h}$ (contact area given mesh size h) onto which the integral of the penalty parameter is evaluated. It is therefore necessary to exploit an iterative procedure, in which at each iteration a solution $p_h^{(k)}$ is first found on the k-th estimated domain $\Omega_{c,h}^{(k)} := \left\{ \mathbf{x} \in \Omega \text{ s.t } \beta(p_h^{(k)}) > 0 \right\}$, secondly updated through a relaxation method with solution $p_h^{(k-1)}$.

The finite element formulation of (2.9)), as proposed in [1], is eventually the following one:
Find $p_h \in Q_h$ s.t.:

$$a(p_h, q_h) + \frac{1}{\epsilon} b(\beta(p_h), q_h) = (f, q_h) \quad \forall q_h \in Q_h. \tag{3.1}$$

An initial value $p_h^{(0)}$ of the iterative method can be extracted from the discretized version of equation (2.3):

$$a(p_h^{(0)}, q_h) = (f, q_h) \quad \forall q_h \in Q_h. \tag{3.2}$$

The intermediate solution $\hat{p}_h^{(k+1)}$ is found solving

$$a(\hat{p}_h^{(k+1)}, q_h) + \frac{1}{\epsilon} \int_{\Omega_{c,h}^{(k)}} \nu(\hat{p}_h^{(k+1)} - \psi) q_h = (f, q_h) \quad \forall q_h \in Q_h. \tag{3.3}$$

Eventually the solution $p_h^{(k+1)}$ is build through a relaxation step:

$$p_h^{(k+1)} = (1-\eta)p_h^{(k)} + \eta\hat{p}_h^{(k+1)} \tag{3.4}$$

with $\eta \in (0,1]$.

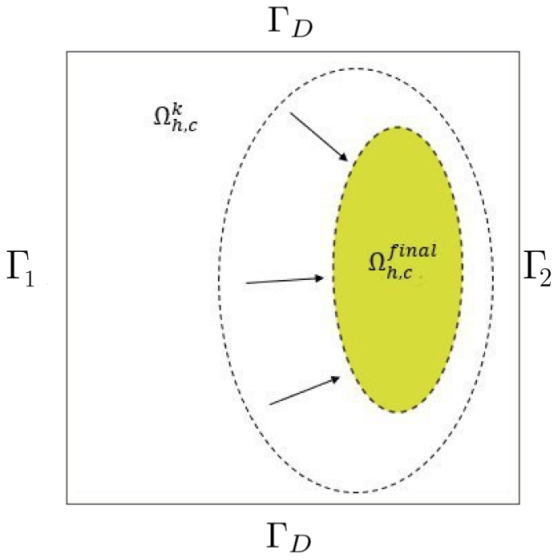

Figure 6: Iterating contact area

3.2 Algebraic formulation

Set ϕ_i as the basis functions spanning Q_h and by $\mathbf{A} \in \mathbb{R}^{n\times n}$ and by $\mathbf{B}^{(k)} \in \mathbb{R}^{n\times n}$ the matrices

$$A_{ij} = a(\phi_j, \phi_i) \qquad \text{and} \qquad B_{ij}^{(k)} = \int_{\Omega_{c,h}^{(k)}} \nu\phi_j\phi_i$$

let moreover $\hat{\mathbf{p}}^{(k)}$, $\mathbf{f}$ and $\boldsymbol{\psi}$ be the vectors corresponding respectively to $\hat{p_h}^{(k)}$ and to the projection of f and ψ on Q_h, then equation (3.3) and (3.4) will now read as follows:

$$\mathbf{A}\hat{\mathbf{p}}^{(k+1)} + \frac{1}{\epsilon}\mathbf{B}^{(k)}\hat{\mathbf{p}}^{(k+1)} = \mathbf{f} + \frac{1}{\epsilon}\mathbf{B}^{(k)}\boldsymbol{\psi} \tag{3.5}$$

$$\mathbf{p}^{(k+1)} = (1-\eta)\mathbf{p}^{(k)} + \eta\hat{\mathbf{p}}^{(k+1)}. \tag{3.6}$$

The computation of a residual is moreover needed to introduce a stopping criterion $|\mathbf{r}| \leq tol$ (where tol is a given tolerance):

$$\mathbf{r} := \mathbf{A}\mathbf{p}^{(k+1)} + \frac{1}{\epsilon}\mathbf{B}^{(k+1)}\mathbf{p}^{(k+1)} - \mathbf{f} - \frac{1}{\epsilon}\mathbf{B}^{(k+1)}\boldsymbol{\psi}. \tag{3.7}$$

3.3 Error estimate

As far as convergence results are concerned, known results have been used within this reference case, i.e. the following lemma holds valid for the *variational inequality problem:*

Lemma 1. *Let $p \in Q$, $p_h \in Q_h$ be solutions of (2.9) and (3.1) respectively. Given a penalty parameter $\epsilon > 0$, the following estimate holds:*

$$||p - p_h||_1 + \epsilon^{-\frac{1}{2}}||\beta(p) - \beta(p_h)||_0 \leq C(h + h^2\epsilon^{-\frac{1}{2}})||f||_0 \tag{3.8}$$

with $C > 0$.

It has been proven furthermore that the best convergence result has been achieved by setting $\epsilon = \mathcal{O}(h^2)$, thus (3.8) reduces to:

$$||p - p_h||_1 \leq Ch||f||_0. \tag{3.9}$$

For detailed derivation of error estimates see [6].

4 MATLAB and algorithms implementation

4.1 Boundary conditions

For this reference case the main boundary conditions to deal with are Dirichlet and periodic ones: the former for the area where lubricant is in contact with air, whereas the latter are needed to recover periodicity information while mapping form cylindrical to Cartesian coordinates.
As far as Dirichlet boundary conditions are concerned, it is simply a matter of finding indexes connected to coordinates of the domain part of interest. The value of the rows, corresponding to the above mentioned indexes, of the **A** matrix (where **A** includes stiffness matrix and penalty operator matrix **B**, see equation 3.5) are set to 0, but the value of the column corresponding to the same row index, that is instead set to 1. The same row index of the rhs is set to 0

$$\begin{bmatrix} a_{11} & a_{12} & a_{13} & a_{14} \\ a_{21} & a_{22} & a_{23} & a_{24} \\ 0 & 0 & 1 & 0 \\ a_{41} & a_{42} & a_{43} & a_{44} \end{bmatrix} \begin{bmatrix} x_1 \\ x_2 \\ x_3 \\ x_4 \end{bmatrix} = \begin{bmatrix} b_1 \\ b_2 \\ 0 \\ b_4 \end{bmatrix}.$$

One last remark has to be brought about when dealing with periodic points. Indeed an algorithm to fix the actual code, from which the present reference study has started, needed to be introduced. When looking for periodic points inside the coordinates vector, the fact that the connectivity matrix was not geometrically ordered, i.e. there was no physical match with the domain, needed to be taken in consideration: consecutive vector indexes did not correspond to consecutive domain points. One way to curb this issue is to implement an algorithm that first sorts the coordinates by values and then rearranges their corresponding indexes into a new vector such that the result is as in Figure 7b. Concerning the implementation of the periodic boundary conditions, the above mentioned indexes are used to find the rows whose values cannot be simply set to zero, since being linear system non homogeneous information would be consequently lost. In order to avoid this, before setting the values of the rows corresponding to the left hand side periodic points to zero, information has to be transferred on the row corresponding to the row of the respective right hand side periodic point. Column indexes of the same

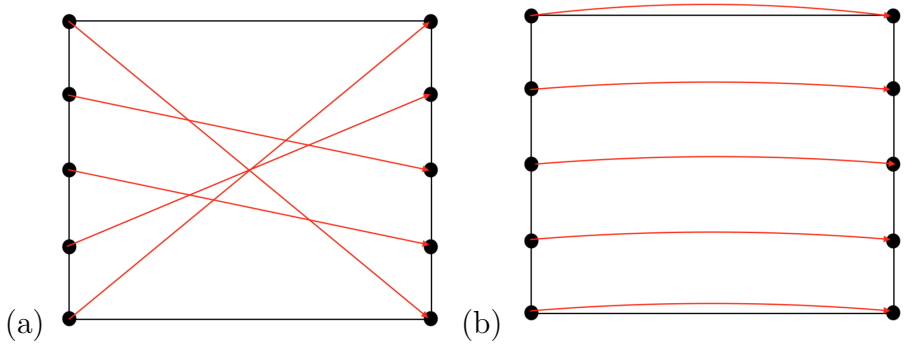

Figure 7: Mismatching (a) vs matching (b) periodic points

periodic points have to be set equal to 1 and -1.

$$\begin{bmatrix} a_{11}+a_{31} & a_{12}+a_{32} & a_{13}+a_{33} & a_{14}+a_{34} \\ a_{21} & a_{22} & a_{23} & a_{24} \\ -1 & 0 & 1 & 0 \\ a_{41} & a_{42} & a_{43} & a_{44}. \end{bmatrix} \begin{bmatrix} x_1 \\ x_2 \\ x_3 \\ x_4 \end{bmatrix} = \begin{bmatrix} b_1+b_3 \\ b_2 \\ 0 \\ b_4 \end{bmatrix}.$$

4.2 Penalty operator

The main issue regarding the implementation of the penalty operator is to understand how to restrict its action to a part of the domain. Indeed at each iteration the penalty operator acts only on the nodes whose pressure value is below the one of the obstacle on those nodes. This is numerically enforced acting on the trial functions, setting therefore the values of the columns of the penalty operator matrix $\mathbf{B}$ equal to zero.

$$\begin{bmatrix} b_{11} & b_{12} & 0 & b_{14} \\ b_{21} & b_{22} & 0 & b_{24} \\ b_{31} & b_{32} & 0 & b_{34} \\ b_{41} & b_{42} & 0 & b_{44} \end{bmatrix}$$

In this way, adding $\mathbf{B}$ to the stiffness matrix, will result in pressure values, of only the nodes relative to the indexes of the trial functions not set to zero, lifted up to the obstacle level.

5 Numerical results

5.1 Reference case of study

In the bearing application considered in this case of study, cf.[1], the following parameters and force function have been chosen. As far as eccentricity between the bearing and the journal is concerned, the film thickness function of variable x is:

$$D(x) = C(1 + \lambda \cos x), \;\; x \in [0, 2\pi], \;\; C > 0$$

where $\lambda \in [0, 1]$ is the eccentricity ratio which depends on the load applied to the bearing. Other parameters used for non-dimensional analysis come instead from experimental measurements:

$$\lambda = 0.4, \;\; C = 12 \cdot 10^{-6}, \;\; L_x = 0.128 \; m, \;\; U = 10 \; m/s, \;\; D_* = 17 \; \mu m.$$

Viscosity is taken equal to 0.1 $Pa \cdot s$, a typical value for motor oils, while the cavitation pressure of the fluid is assumed equal to the atmospheric pressure, therefore the obstacle function is set as the reference pressure: $\psi = 0$. Figure 8 shows the solution of the main problem without obstacle in a square domain Ω.

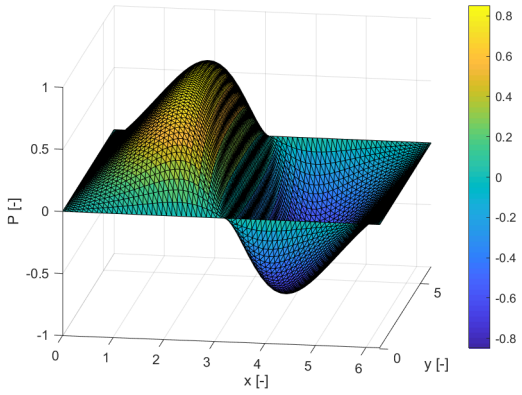

Figure 8: Solution without penalty operator for nRef[1]=6

[1]nRef is the number of refinements of the mesh

5.2 Cavitation area

Introducing the penalty operator, by setting $\epsilon = h^2$, the square domain Ω is consequently subdivided into a contact-free and a contact area

$$\Omega_f := \{x \in \Omega \text{ s.t. } p(x) > 0\}$$

$$\Omega_c := \{x \in \Omega \text{ s.t. } p(x) = 0\}$$

respectively. For different mesh sizes, plots of the solution are presented in Figure 9.

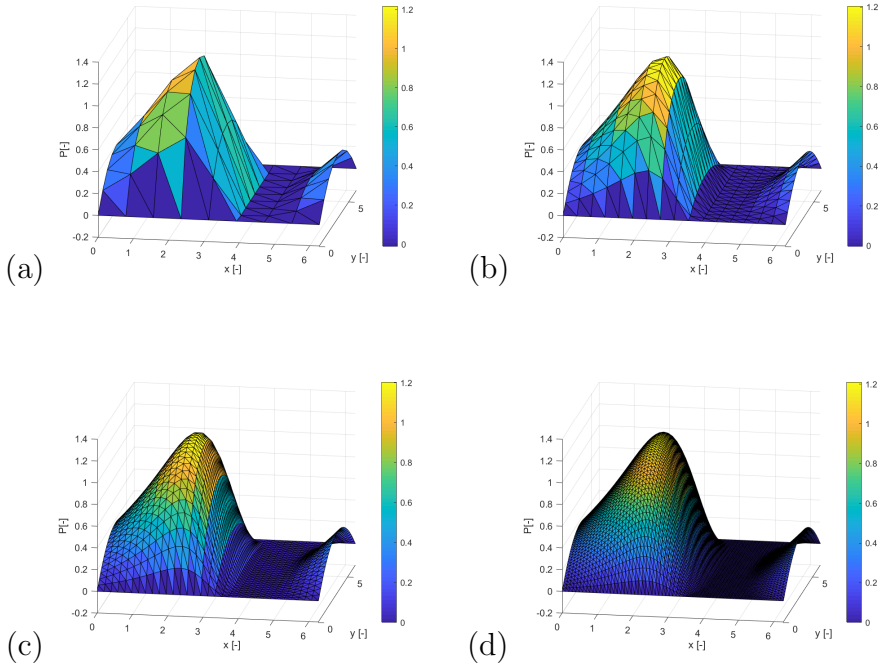

Figure 9: Solution plots for (a) nRef=3, (b) nRef =4, (c) nRef=5, (d) nRef=6

As shown in Figure 9, the obstacle operator works as expected by theory, lifting up the negative area identified in Figure 8. To better analyze the cavitation area, Figure 10 shows the evolution of negative values (in red) until convergence. These results have been obtained setting $\eta = 0.95$ and the stopping criteria $tol = 10^{-8}$. In Table 1 are shown numbers of iteration for different values of nRef.

nRef	3	4	5	6
niter	10	12	15	20

Table 1: nRef vs Number of iterations

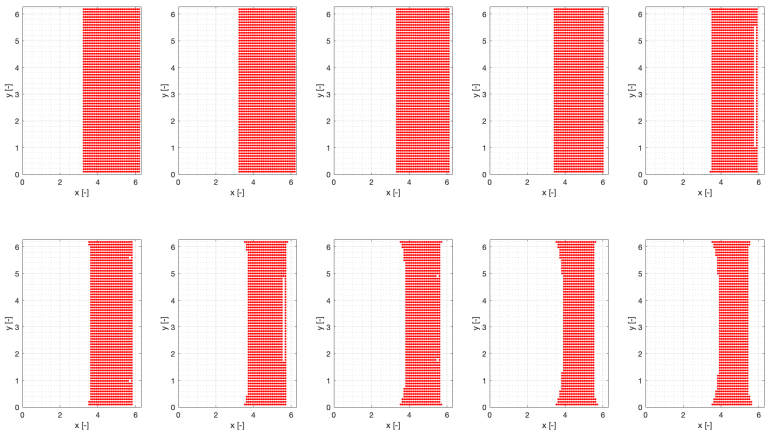

Figure 10: Evolution of cavitation area for nRef=6

5.3 Convergence

5.3.1 Numerical analysis

Due to the fact that an exact solution of the proposed problem is not available, a first way to analyze the convergence of the method is to use a numerical solution with very small values of h ($nRef = 8$) as an exact solution. Obviously the error estimated in equation (3.9) has to be evaluated in the finer mesh: it is necessary to add pressure values on non existent nodes in the coarser mesh, exactly where nodes of finer mesh are located. A growing nRef implies a higher number of nested meshes, so that through linear interpolation methods, it is possible to determine the required values of the pressure onto the corresponding finer mesh nodes. By definition of H^1 norm

$$||\cdot||_1^2 = ||\cdot||_0^2 + ||\nabla(\cdot)||_0^2,$$

the required norm of equation (3.9) becomes:

$$||e||_1 = \sqrt{e^T \mathbf{A} e + e^T \mathbf{M} e} \tag{5.1}$$

denoting with $e = p - p_h$ and with $\mathbf{A}$ and $\mathbf{M}$ the stiffness and the mass matrix.
In Figure 11 it is shown the linear convergence ($\epsilon = h^2$), as expected by theoretical results of equation (3.9).

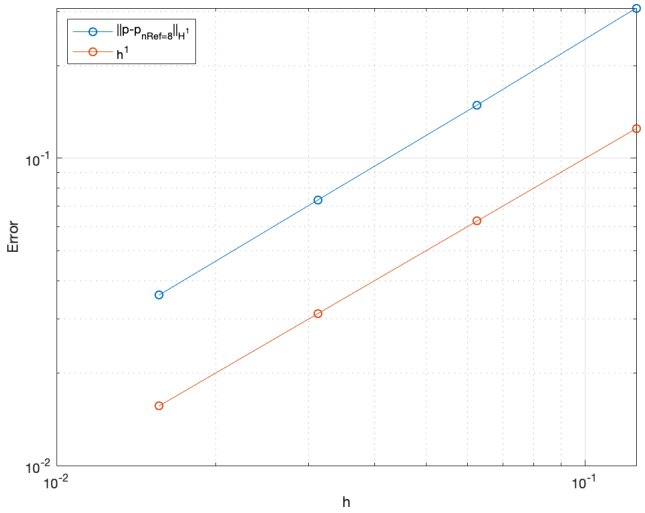

Figure 11: Numerical convergence result

5.3.2 Exact solution problem and robustness analysis

A further way to prove convergence results stated among numerical results, is to test the penalty operator with a different problem, with different boundary conditions (in this case Dirichlet and Neumann) whose exact solution is instead known, cf.[6]: so that result (3.9) can be used straightforward to check whether results are consistent with those obtained in the previous subsection. The full equation of the exact solution problem chosen for this study is the following:

$$-\Delta p \geq 0 \text{ and } p \geq \psi \text{ in } \Omega$$

where $\Omega = (-1, 1) \times (0, 1)$ and the obstacle is defined as

$$\psi(x, y) = 1 - 4x^2. \tag{5.2}$$

Boundary conditions are

$$p(-1,y)=0,\;\; p(1,y)=0,\;\; \frac{\partial p(x,0)}{\partial n}=0,\;\; \frac{\partial p(x,1)}{\partial n}=0,\;\; \text{on } \partial\Omega.$$

The analytical solution to the problem is

$$p(x,y)=\begin{cases}\frac{1-4x_0^2}{x_0-1}(x-1), & x\in[-1,-x_0]\\ 1-4x^2, & x\in[-x_0,x_0]\\ \frac{1-4x_0^2}{1-x_0}(x+1), & x\in[x_0,1]\end{cases}$$

with $y\in[0,1]$, where $x_0=1-\sqrt{3}/2$.
Aim of the penalty operator in this situation is to lift pressure above a value not constant, as in the reference case of study, but varying over the domain according to the obstacle function (5.2).

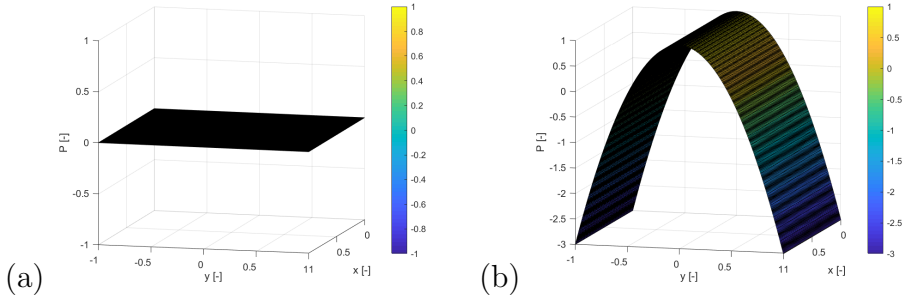

Figure 12: nRef=6 (a) Solution not lifted; (b) Obstacle function

Penalty operator works properly in this case as well, lifting up, with continuity, the whole initial solution, reaching at convergence an almost prefect matching with the exact one as Figure 13 shows.
Using an exact solution problem has allowed a deeper study of convergence properties, as far as its evaluation for different values of epsilon is concerned. Indeed Figure 14 presents convergence results that not only confirmed those obtained in the previous subsection, but supply further information on convergence letting parameter epsilon varying.
It is inferable from Figure 14 that $\epsilon = h^2$ provides the best convergence results, not only for lower magnitude value of penalty parameters but also for higher values: a stronger penalty parameter in fact results into a much higher amount of iteration needed for convergence as Table 2 shows (nRef=6).

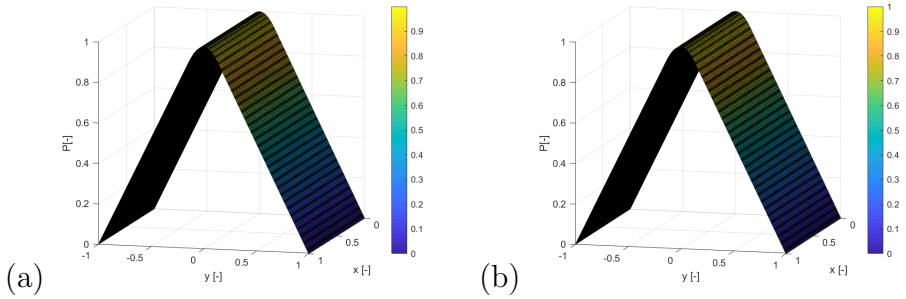

Figure 13: nRef=6 (a) Numerical solution; (b) Exact solution

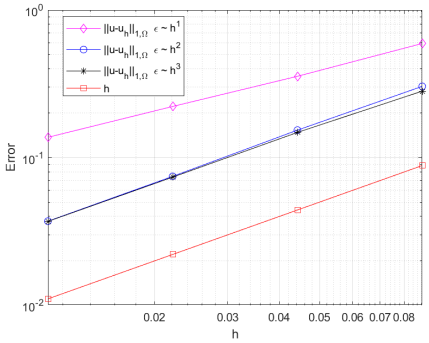

Figure 14: Convergence results for different ϵ

ϵ	h^2	h^3	h^4	h^5
niter	20	28	89	200+

Table 2: ϵ vs number of iterations

Testing penalty operator algorithm is not only useful to double check convergence results, but more relevantly to test algorithm robustness, flexibility and correctness while seeing it working successfully for different and more challenging problems.

5.4 Errors

A last numerical result that is important to emphasize, concerns the analysis of incremental error and pointwise convergence of the cavitation area, as far as the main differential problem proposed as case of study within this report

in chapter 5.1 (cf. [1]) is considered. Using numerical tools, an exact value of the cavitation pressure is not obtainable, nevertheless it is essential to ensure that the value of pressure in the cavitation area is converging pointwise to zero as number of refinements increase.

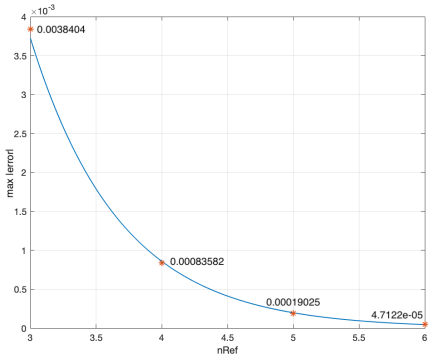

Figure 15: Pointwise convergence of maximum absolute error value

In figure 15, the maximum value of the pointwise error is shown to converge to zero as expected.

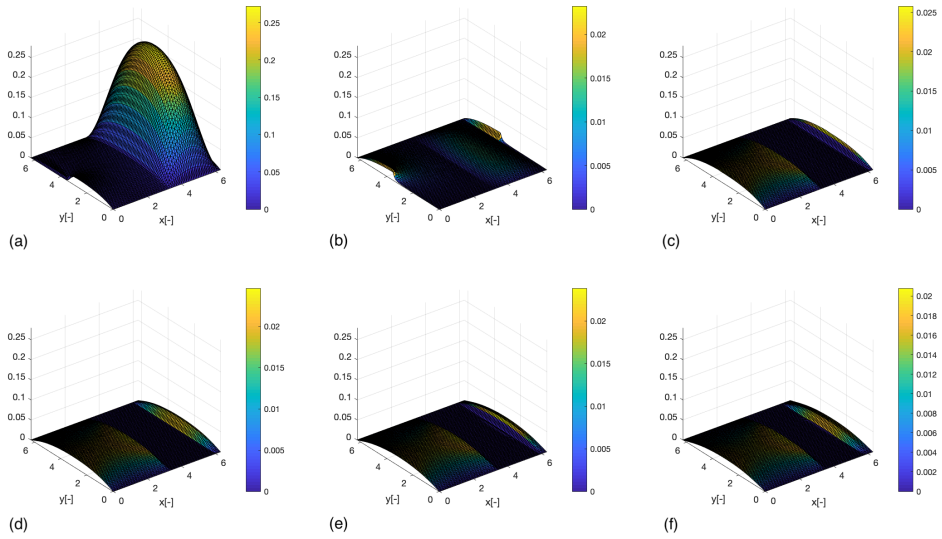

Figure 16: Incremental error (a)-(f) number iteration 1 - 7

As far as incremental error is instead concerned, Figure 16 shows that areas

where the penalty operator does not act exhibit a lower initial incremental error. The overall result is anyway consistent with the expected pointwise convergence already at 7th iteration (nRef=6).

6 Conclusions

The main goal of the report was to propose a way to model cavitation phenomenon, starting from Navier-Stokes equation and introducing further admissible simplifications. The obtained results were not consistent with the experimental data and the physical phenomenon itself. A way to curb this issue was to improve the model both introducing a *variational inequality problem* and subsequently an *obstacle problem*: in this way the non physical negative values of pressure were lifted up so to reach physical consistency with cavitation phenomenon.
Nevertheless further improvements of the numerical model are possible, in order to give more detailed an precise description of the evolution of the cavitation area, as well as to improve numerical convergence. As far as the first above mentioned issue is concerned, unstructured or adaptive mesh approach could be used to obtain further information at the interface of the contact area. Whereas instead, when dealing with numerical issues, instabilities connected to large eigenvalues differences for ϵ penalty parameter going to zero can be smoothed introducing an augmented Lagrangian method, where convergence of Lagrange multipliers leads to convergence of the method without necessarily implying convergence to zero of the penalty parameter. Discontinuous Galerkin method could be moreover used instead of the Continuous one.
A final remark can be done to introduce a different numerical method to spot cavitation area instead of the penalty one. Using in fact Karush-Kuhn-Tucker (KKT) optimality conditions, whose methodology is explained in [5], inequality constraint $p \geq \psi$ are forced into the main equation Lagrange function and its spatial gradient is taken equal to zero:

$$\mathbf{Aq} - \mathbf{f} - \boldsymbol{\lambda} = \mathbf{0}$$

$$\mathbf{q} - \boldsymbol{\psi} \geq \mathbf{0}$$

$$\boldsymbol{\lambda} \geq \mathbf{0}$$

$$\boldsymbol{\Lambda}(\mathbf{q} - \boldsymbol{\psi}) = \mathbf{0}$$

where $\boldsymbol{\lambda}$ is the Lagrange multiplier vector and $\boldsymbol{\Lambda}$ is the diagonal matrix of Lagrange multipliers.
Introducing moreover the slack vector $\mathbf{s} := \mathbf{q} - \boldsymbol{\psi}$ and the matrix of slack

vectors $\mathbf{S}$, it is possible to solve the above mentioned equation using Newton method in search of optimal points:

$$\begin{bmatrix} \mathbf{A} & -\mathbf{I} & 0 \\ -\mathbf{I} & 0 & \mathbf{I} \\ 0 & \mathbf{S} & \mathbf{\Lambda} \end{bmatrix} \begin{bmatrix} \delta\mathbf{q} \\ \delta\boldsymbol{\lambda} \\ \delta\mathbf{s} \end{bmatrix} = - \begin{bmatrix} \mathbf{Aq} - \mathbf{f} - \boldsymbol{\lambda} \\ \mathbf{s} - (\mathbf{q} - \boldsymbol{\psi}) \\ \mathbf{\Lambda S1} \end{bmatrix} \tag{6.1}$$

where $\mathbf{1}$ is a vector of ones.
It has been proven (cf.[6]) that KKT model supplies a more accurate evaluation of the cavitation area, even though computational wise system (6.1) is strongly ill conditioned, so that more detailed studies of matrix preconditioning have to be carried out.

References

[1] Sorsimo A., Juntunen M., Stenberg R. and Videman J. *Finite Element Analysis of the Reynolds Lubrication Equation with Cavitation.* Journal of Structural Mechanics, 2012.

[2] Kinderlehrer D., and Stampacchia G. *An Introduction to Variational Inequalities and Their Applications.* Society for Industrial Mathematics, 1987.

[3] Johnson C. *Adaptive Finite element methods for the obstacle problem.* Mathematical Models and Methods in Applied Sciences 2, 1996.

[4] Harrison O. J. *The Hydrodynamical Theory of Lubrication with special Reference to Air as Lubricant.* Cambridge : Univ. press, 1913.

[5] Nocedal J., Wright S. *Numerical Optimization.* Springer, 2000.

[6] Sorsimo A., *Solution of the inequality constrained Reynolds equation by the finite element method.* Master's thesis, Aalto University School of Science. 2012.